

Experimental and theoretical evidences of p-type conductivity in nickel carbodiimide nanoparticles with a delafossite structure type

Tengfei Jiang, Baptiste Polteau, Yoann Farré, Laurent Cario, Camille Latouche, Yann Pellegrin, Mohammed Boujtita, Fabrice Odobel, Franck Tessier, François Cheviré, et al.

▶ **To cite this version:**

Tengfei Jiang, Baptiste Polteau, Yoann Farré, Laurent Cario, Camille Latouche, et al.. Experimental and theoretical evidences of p-type conductivity in nickel carbodiimide nanoparticles with a delafossite structure type. Inorganic Chemistry, 2017, 56 (14), pp.7922-7927. 10.1021/acs.inorgchem.7b00636 . hal-01559094

HAL Id: hal-01559094
https://hal.science/hal-01559094

Submitted on 10 Jul 2017

HAL is a multi-disciplinary open access archive for the deposit and dissemination of scientific research documents, whether they are published or not. The documents may come from teaching and research institutions in France or abroad, or from public or private research centers.

L'archive ouverte pluridisciplinaire **HAL**, est destinée au dépôt et à la diffusion de documents scientifiques de niveau recherche, publiés ou non, émanant des établissements d'enseignement et de recherche français ou étrangers, des laboratoires publics ou privés.

Experimental and theoretical evidences of *p*-type conductivity in nickel carbodiimide nanoparticles with a delafossite structure type

Tengfei Jiang[*a, b], Baptiste Polteau[c], Yoann Farré,[d] Laurent Cario[a], Camille Latouche[a], Yann Pellegrin,[d] Mohammed Boujtita,[d] Fabrice Odobel[d], Franck Tessier[c], François Cheviré[*c] and Stéphane Jobic[*a]

[a]Institut des Matériaux Jean Rouxel (IMN), Université de Nantes, CNRS, 2 rue de la Houssinière, BP 32229, 44322 Nantes, Cedex 03, France

[b]School of Chemistry and Chemical Engineering, Yangzhou University, 180 Siwangting Road, Yangzhou, 225002, P. R. China

[c]Institut des Sciences Chimiques de Rennes (UMR CNRS 6226), Université de Rennes 1, 263 avenue du Général Leclerc, 35042 Rennes Cedex, France

[d] Université LUNAM, Université de Nantes, CNRS, Chimie et Interdisciplinarité: Synthèse, Analyse, Modélisation (CEISAM), UMR 6230, 2 rue de la Houssinière, 44322 Nantes cedex 03, France

ABSTRACT: Nickel carbodiimide ($NiCN_2$) was synthesized using a two-step precipitation-decomposition route leading to a brown powder with gypsum flower-like morphology and a large specific surface area (75 m^2/g). This layered material crystallizes in the 2H structure type of delafossite (SG = $P6_3/mmc$) which is built upon infinite $^2/_\infty[NiN_2]$ layers connected by linear carbodiimides bridges $[N=C=N]^{2-}$. A XRD Rietveld refinement, as well as thermal analyses, tends to point out some nickel deficiencies in the material, and band structure calculations carried out on the defect compound predict *p*-type conductivity in relation to a slight amount of N^{2-}. This *p*-type conductivity is demonstrated by electrochemical impedance spectroscopy measurements, and a flat band potential of 0.90 V vs. SCE at pH of 9.4 is measured. This value, which is more positive than that of $CuGaO_2$ and $CuCrO_2$ delafossite oxides and NiO, prompts us to test $NiCN_2$ nanoparticles as a photocathode in *p*-type dye sensitized solar cells (*p*-DSSCs).

INTRODUCTION

Delafossite materials are well known layered ternary compounds that attracted a renewed interest when Kawazoe et al. underscored the capability of $CuAlO_2$ films to exhibit both a *p*-type conductivity and a high optical transparency.[1] This discovery opened up the door to numerous investigations that ended up at applications in the field of optoelectronic devices,[2] diodes,[3] and solar cells.[4] Namely, $A^+B^{3+}O_2$ delafossite structure (e.g. A = Cu, Ag, Pd, Pt; B = Cr, Fe, Co, Cu, Al, Ga, In, Y, Rh) can be described as built upon $^2/_\infty[BO_2]$ layers consisting of edge-sharing $[BO_6]$ octahedra layers. These 2D blocks are perpendicularly connected to each other via O-A-O dumbells.[5] According to the stacking of the anions (aa bb cc or aa bb), two different crystal configurations, labelled 3R and 2H (R-3m and $P6_3/mmc$ space groups, respectively) can be observed.[6] Naturally, these structure types accept a slight deviation from the 1:1:2 stoichiometry, what explains their electrical behavior. Commonly, oxygen at interstitial sites and/or monovalent cations off-stoichiometry are put forward to account for the observed *p*-typeness in these materials.[7] Possible substitutions on the A and B sites may help to adjust the carrier concentration,[8] while the oxygen over-stoichiometry may be modulated via topotactic reduction what strongly affects both the flat band potential, (i.e. the position of the last occupied state in energy), and the concentration of free carriers.[9]

Actually, delafossite structures are not limited at all to oxides. A few ABN_2 nitride materials, prepared by a cationic exchange reaction from $NaBN_2$, exhibit also this structure type with A^+ and B^{5+} cations (e.g. A = Cu, Ag; B = Nb, Ta)[10,11,12]. This series can also be extended to MNCN carbodiimides (e.g. M = Mn, Fe, Co, Ni) even if their initial description did not spotlight this filiation. In these MCN_2 compounds, M^{2+} transition elements and C^{4+} cations are sixfold and twofold coordinated, respectively.[13, 14, 15, 16] If the magnetic properties of $MnCN_2$, $FeCN_2$, $CoCN_2$ and $NiCN_2$ have been investigated (antiferromagnets below 30 K, 345 K, 255 K, and 360 K, respectively), their conductive behavior, a property of capital importance in view of potential (photo)-electrical applications[17], is not reported yet. In that framework, based on the new interest for delafossite materials in the field of *p*-type dye sensitized solar cells (*p*-DSSCs), we embarked first on the elucidation of the conductivity type of the $NiCN_2$ compound by electrochemical impedance spectroscopy measurements,

then on the setting up of a $NiCN_2$ based solar cell. Indeed, $NiCN_2$ could appear *prima facie* as an alternative to NiO, the most commonly used *p*-type material for the aforementioned application.[18, 19, 20, 21, 22, 23] Both compounds are described as charge transfer insulators in their stoichiometric form and $^2/_\infty[NiN_2]$ layers strongly resemble to $^2/_\infty[NiO_2]$ layers (the ones condense along the <111> axis in NiO to give rise to the tridimensional NaCl structure type).[24, 25, 26]

EXPERIMENTAL SECTION

Synthesis. The synthesis of $NiCN_2$ nanoparticles powder was adapted from literature.[15,27] First, the $Ni(HNCN)_2$ precursor was precipitated overnight from a dark blue solution of $Ni(NH_3)_6^{2+}$ complex and $[NCN]^{2-}$ anions obtained by dissolution of 2.08 g of $Ni(NO_3)_3 \cdot 6H_2O$ and 1.5 g of H_2CN_2 in 30 ml of a 12.5 Vol% ammonia solution. The green precipitate was isolated by centrifugation, rinsed with distilled water and dried under vacuum overnight at room temperature. Second, the precursor was thoroughly ground in an agate mortar with a KCl/LiCl mixture (54/46 molar ratio, $T_{Eutectic}$ = 352 °C)[28] in a one by one weight ratio, and fired in an alumina boat under flowing nitrogen at 330 °C overnight, before heating at 400 °C for 24 h. The as-prepared product was finally washed several times with distilled water to get rid of alkali chlorides. The product was centrifuged and dried under vacuum for several days at room temperature. The obtained powder is dark brown (Figure S1).

X-ray diffraction. X-ray diffraction (XRD) data were recorded at room temperature in the 2θ range 5-120° with a step size of 0.026° and a scan time per step of 400 s using a PANalytical X'Pert Pro diffractometer (Cu *K-L2,3* radiation, PIXcel 1D detector, Data Collector software). The Rietveld refinement for $NiCN_2$ was carried out with the Fullprof program[29] considering the $P6_3/mmc$ space group (n°194). The Pseudo-Voigt profile function was used and the background was approximated by linear interpolation between a set of background points (23). Profile and atomic parameters were refined considering full site occupancy for atoms except for the Ni 2*a* position. Standard deviations (ESD) were corrected using the Berar and Lelann coefficient calculated from the structure refinement.[30, 31] Results of the refinement are gathered in Table S1 and S2.

Thermal analyses. Thermogravimetric and Differential Scanning Calorimetry (DSC) measurements were conducted with a Jupiter STA 449 F3 instrument in air from room temperature to 800 °C with a heating rate of 2 °C/min.

Scanning electron microscopy. Scanning electron microscopy micrographs were collected on a JEOL7600F apparatus on powder spread on a carbon tape pasted over a copper metal sample holder.

Specific surface area. Specific surface areas were obtained by Brunauer–Emmett–Teller (BET) analyses done in a micrometrics ASAP 2010 analyser.

Electrochemical impedance spectroscopy (EIS) measurements. $NiCN_2$ powders were pressed under 100 bars to generate hard pellets. Carbon paste was painted on one side to make the back contact between $NiCN_2$ pellet and copper wire. Then the pellet was embedded in a resistant epoxy glue. Before EIS measurement, the surface of $NiCN_2$ pellet was polished by SiC paper to get a mirror-like smooth surface. EIS measurements were then carried out with an electrochemical workstation (SP-300, Biologic Sciences Instruments). The electrolyte is a 1 M $LiClO_4$ aqueous solution (pH = 9.4), and a platinum electrode and a saturated calomel electrode (SCE) were used as counter and reference electrode, respectively.

Preparation of the $NiCN_2$ photocathode and fabrication of p-DSSC. The $NiCN_2$ film was prepared by the screen printing method. First 100 mg of $NiCN_2$ powder was ball milled with 3 mL ethanol. Second the mixture was dropped into a mixed solution with 3 mL ethanol, 1 mL terpineol, and 1 mL 5% ethyl cellulose solution in ethanol under stirring. After 15 min, the ethanol was removed by using rotary evaporator. A layer of $NiCN_2$ paste was then coated on a FTO glass. The as-prepared film, after sintering at 350°C in air for only 10 min (to avoid its degradation (Figure S2)), was dipped into a 0.2 mM of a diketopyrrolopyrrole based dye[32] (Figure S3) solution ((1:1) ethanol/dichloromethane) for 24 h at room temperature. The counter electrode was prepared by chemical deposition of platinum from 2 mg/mL hexachloroplatinic acid solution in isopropanol. A thin transparent film of Surlyn polymer (DuPont, 25 µm) was placed between the photocathode and the Pt electrode as a spacer to form the electrolyte space and both electrodes were sealed by heating the edges at 200 °C. The electrolyte is 0.1 M tris(4,4'-bis-tert-butyl-2,2'-bipyridine) cobalt (III/II)[33] (Figure S4) and 0.1 M $LiClO_4$ in propylene carbonate. The active area of the cell is 0.25 cm^2.

Characterization of the $NiCN_2$ based p-DSSCs. The photocurrent-photovoltage characteristics were measured using a Keithley model 2400 digital source meter. The solar simulator is an Oriel Lamp calibrated to 100 mW/cm^2. The overall conversion efficiency (η) of the photovoltaic cell is calculated from the integral photocurrent density (J_{sc}), the open-circuit photovoltage (V_{oc}), the fill factor of the cell (FF), and the intensity of the incident light.

Electronic structure calculations. The electronic structure of the system has been investigated using quantum calculations with the VASP program.[34] Calculations have been performed on a perfect 64 atoms supercell, formally $Ni_{16}C_{16}N_{32}$. In order to get insights on the electric behavior of the material, the defected cell, which contains a Ni vacancy, was studied with the $Ni_{15}C_{16}N_{32}$ composition. Both structures were optimized at the GGA level. DOS were simulated at the same level and using the global hybrid PBE0 functional.[35, 36] Density of States were analyzed using the PyDEF software.[37]

RESULTS AND DISCUSSION

Rietveld refinement of the XRD pattern (Figure 1) confirms the crystallization of $NiCN_2$ according to the 2H structure of delafossite as reported by Krott et al.[15] Refined lattice parameters, nitrogen *z* position, isotropic atomic displacements and the occupancy rate of the 2a site by Ni are gathered in Tables S1 and S2. Overall data are in good agreement with those reported in the literature. Nevertheless, the chemical formulation issued from the X-ray analysis, $Ni_{0.88(3)}CN_2$, suggests a Ni off-stoichiometry and the possible existence of a Ni^{2+}/Ni^{3+} mixed valence to balance the charges.

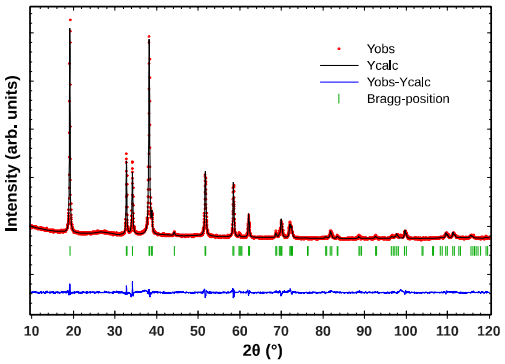


Figure 1. Rietveld refinement of the $NiCN_2$ diagram in the *P6₃/mmc* hexagonal space group.

The crystal structure of $NiCN_2$ is displayed in Figure 2 and clearly highlights the affiliation of the material to the delafossite structure type with linear carbodiimides groups $[N^{=}C^{=}N]^{2-}$ separating the $^{2}/_{\infty}[NiN_2]$ layers.

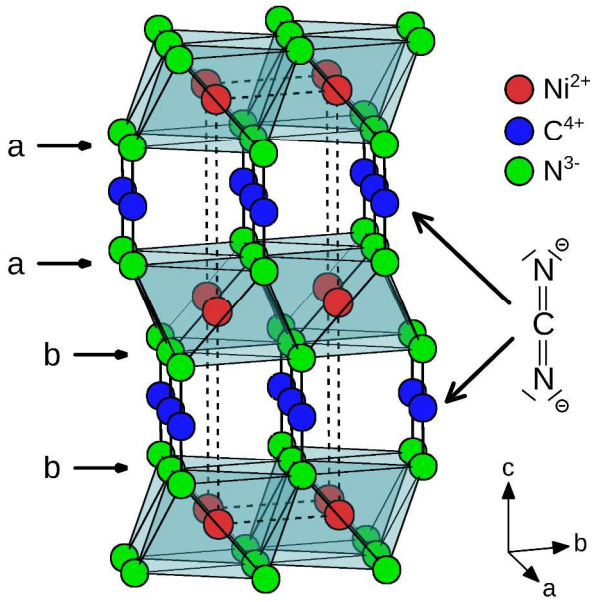


Figure 2. Crystal structure of $NiCN_2$ (SG: *P6₃/mmc*)

The scanning electron microscopy (SEM) images of $NiCN_2$, displayed in Figure 3, reveal an intergrowth of crystalline nanoplates that strongly resembles to gypsum flowers with 20-30 nm thick and 500-600 nm large rose petals. Such a bi-dimensional nanostructured morphology, inherited from the layered character of delafossite structure type, leads to a quite high specific surface area of 75 m^2/g.

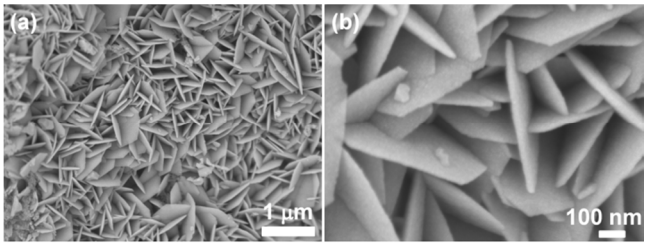


Figure 3. SEM images of $NiCN_2$ nanoparticles at low (a) and high (b) magnification.

The thermal stability in air of $NiCN_2$ was studied by thermogravimetric analysis-differential scanning calorimetry (TGA-DSC). From the examination of Figure 4, it may be suggested that the weight loss observed in the 80-150 °C range (~5%) is associated to the departure of chemisorbed and physisorbed water molecules at the surface of the powdered sample, while the abrupt one at 385 °C (~33%) is due to the endothermic decomposition of $Ni_{0.88(3)}CN_2$ to form NiO. Thermal analysis carried out under nitrogen (not shown here) indicates a similar behavior with decomposition of "$NiCN_2$" into metallic Ni element around the same temperature. Clearly, the TGA analysis reported here fully agrees with a sub-stoichiometry on the Ni site in "$NiCN_2$". This one, estimated around 10% from XRD, would reach about 25% based on the examination of the TGA curve. This difference may originate from weight uncertainties, but also to the existence of a correlation between the scale factor and Ni occupation fraction at the X-Ray pattern refinement step that could minimize the calculated off-stoichiometry. In addition, the platelet shape of thin "NiCN2" crystals (see Figure 3) may favor physisorption phenomena, while the occurrence of N=C=N, N=C=O or even O=C=O pending species at the surfaces can be envisioned for passivation reasons. This may also contribute to the high weight loss observed on the TGA curve.

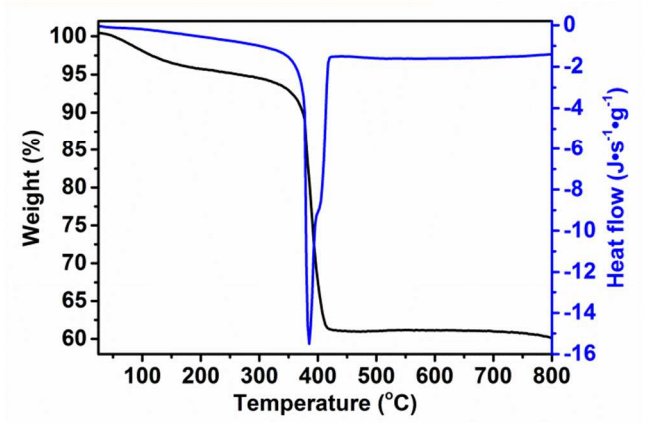


Figure 4. TGA-DSC curves of $NiCN_2$ powder collected under air atmosphere.

The DOS using the PBE0 hybrid functional of the perfect and the defected cell are given in Figure 5, top and middle respectively. As one can see for the ideal structure, the

band-gap is, as expected using such functional, slightly overestimated. This perfect structure possesses the valence band constructed around the N(*p*) orbitals with a non-negligible amount of Ni(*d*) contribution. The bottom of the conduction band is mainly composed of Ni orbitals. Despite this high level of accuracy in the computation (PBE0), it is impossible to explain the *p*-type behavior of the material with a perfect cell. Consequently, the investigation of a defected cell with one missing Ni has been performed. It turned out that, whatever the level of accuracy in the computation (GGA/Hybrid), an acceptor level built upon N atomic orbitals is present near the Valence Band Maximum. Clearly, the electronic density map (Figure 5, bottom, orange) shows that the hole is mainly localized on the two nitrogen atoms of the N=C=N carbodiimide groups surrounding the missing Ni positioned at the supercell corner edges. This result provides a suitable explanation concerning the *p*-type behavior of the studied material, and suggests that a hole localized at the top of the *sp* anionic band has to be privileged over a Ni^{2+}/Ni^{3+} mixed valence to account for the *p*-typeness in $NiCN_2$.

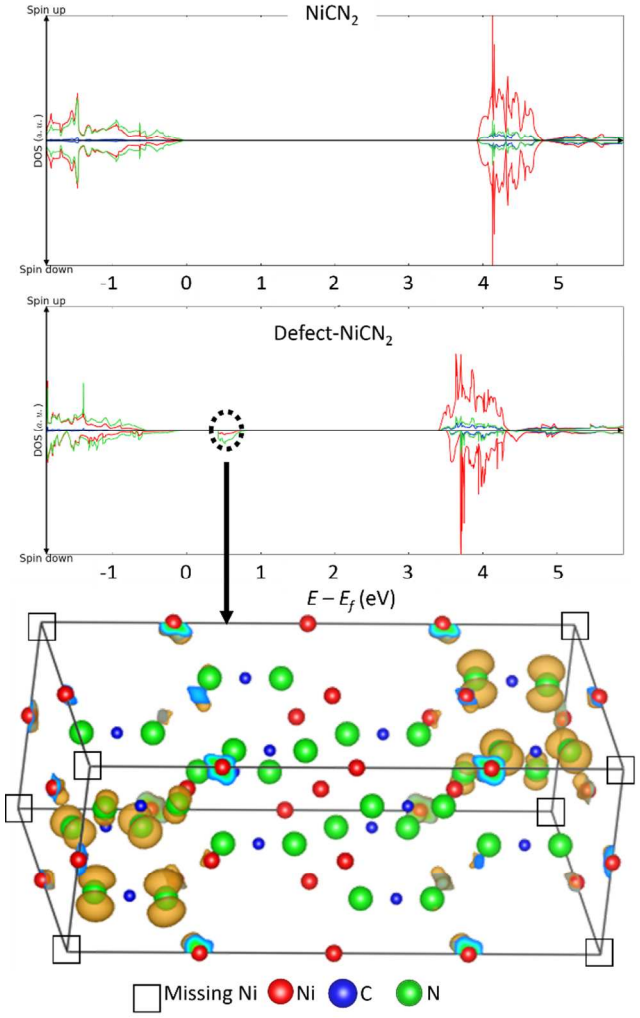


Figure 5. Density of states of perfect (top) and defect (middle) $NiCN_2$ structures, and partial band decomposition charge density of the E_F frontier region including the vacant levels (black circle) localized on the defected structure(bottom). Electronic density in orange and intersection at the limit of the supercell in cyan.

To probe the expected *p*-typeness of deficient NiCN2, electrochemical impedance spectroscopy measurement were carried out on pressed pellet immersed in an electrolyte consisting of a 1 M $LiClO_4$ aqueous solution (pH = 9.4) The flat band potential (V_{FB}) was determined from the intercept of the reciprocal square capacitance axis with the potential axis, based on the Mott-Schottky equation:[38]

$$1/C^2 = (2/e\varepsilon_o\varepsilon N_a)[(V-V_{FB})-kT/e]$$

where C represents the capacitance of the space charge region, ε_o is the vacuum permittivity, ε is the dielectric constant, e is the electron charge, V is the electrode applied potential, k is the Boltzmann constant, T is the absolute temperature, and N_a is the acceptor concentration. The negative slope of Mott-Schottky plots (Figure 6) confirms the *p*-type conductivity of $NiCN_2$ sample. The measured V_{FB} at pH 9.4 is 0.90 V (vs. SCE) for $NiCN_2$. This is more positive than the flat band potential measured for other delafossite oxides (*e.g.* 0.49 V vs. Ag/AgCl at pH 7.2 for $CuAlO_2$,[39] 0.49 V vs. SCE at pH 6.3 for $CuGaO_2$,[40] and 0.50 V vs. SCE at pH 9.4 for $CuCrO_2$[9]), and 0.8 V higher than that of NiO purchased from Inframat and evaluated in

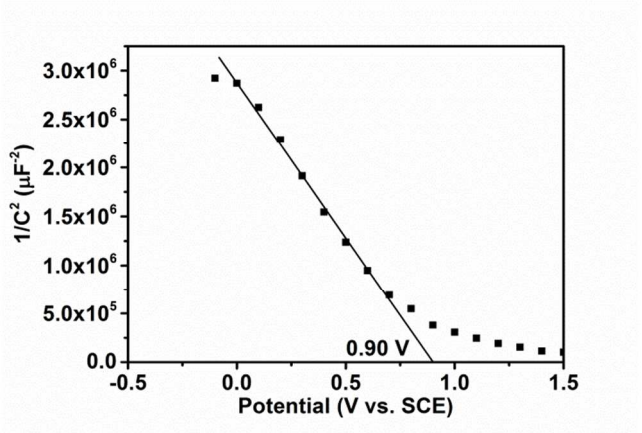


Figure 6. Flat band potential of $NiCN_2$ in 1 M $LiClO_4$ at pH 9.4.

identical conditions.[41] This clearly means that the valence band of $NiCN_2$ is much deeper than that of NiO. As aforementioned, the *p*-typeness would originate from Ni deficiency in the $^2/_\infty[NiN_2]$ layer in contrast with regular delafossite oxide where *p*-type carriers are deemed to be related to defects located between the $^2/_\infty[BO_2]$ layers.

The *p*-type conductivity of $NiCN_2$ concomitant with a deep valence band prompts us to use this material as substitute of NiO in *p*-DSSC. The photovoltaic performances of the solar cells made with $NiCN_2$ photocathode conditions are gathered in Figure 7 and turn to be of very poor performances (η = 0.0073 %). Nevertheless, the setting up of the solar cell fully asserts the capability of the dye to inject holes in "$NiCN_2$" as for NiO, in agreement with the *p*-type character of this new material and the

exergonicity of this reaction albeit weak (ΔG_{inj} = -0.09 eV)[42]. The V_{oc} is of 343 mV that is similar with that of NiO.[32] The low conversion efficiency comes probably from several reasons. First, the amount of grafted dyes at the surface of the photocathode was low, second the injection driving force is relatively small and can preclude to achieving high hole injection quantum yield. Finally, the surface of $NiCN_2$ may not inhibit charge recombination with the electrolyte as confirmed by the current/voltage characteristic recorded in the dark, where the rectifying effect is far from being large (Figure 7). The latter issue most probably explains that we cannot reach high V_{oc} as should permit the deep valence band potential of $NiCN_2$. New dyes substituted with more suitable anchoring groups and displaying higher oxidative power in the excited state would most certainly give higher performances.

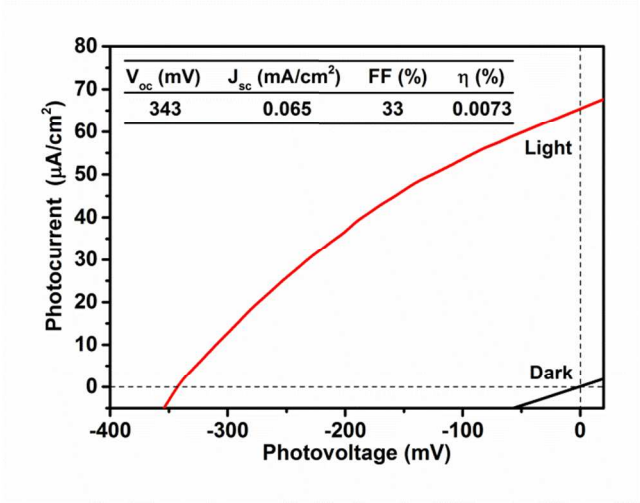


Figure 7. Photovoltage–photocurrent curves under AM 1.5 illumination (1000 W/m²) and dark current curves of solar cells constructed from $NiCN_2$. Inset: the V_{oc}, J_{sc}, FF, and η of the cell.

In summary, we have synthesized nanostructural $NiCN_2$ nanoplates based on a model adapted from Krott et al. and evidenced the *p*-type conductivity of nickel carbodiimide both by capacitance measurements and by the achievement of the first *p*-type dye sensitized solar cell using transition metal carbodiimide. As suggested by band structure calculation *p*-typeness in this delafossite compound would originate from a N^{3-}/N^{2-} mixed valence induced by a slight Ni off stoichiometry.

ASSOCIATED CONTENT

Supporting Information. This material is available free of charge via the Internet at http://pubs.acs.org.

AUTHOR INFORMATION

Corresponding Author

* E-mail: jiangtengfei@yzu.edu.cn; francois.chevire@univ-rennes1.fr; stephane.jobic@cnrs-imn.fr.

Notes

The authors declare no competing financial interest.

ACKNOWLEDGMENTS

TJ, LC, YP, MB, FO, and SJ are grateful to the Agence Nationale de la Recherche for the program POSITIF (No. ANR-12-PRGE-0016-01), for financial support. BP is indebted to CNRS, Universities of Nantes and Rennes 1, and the Bretagne and Pays de la Loire Régions for his PhD funding within the Materials program. CL thanks E. Pean for PyDEF supports.

REFERENCES

(1) Kawazoe, H.; Yasukawa, M.; Hyodo, H.; Kurita, M.; Yanagi, H.; Hosono, H. p-Type Electrical Conduction in Transparent Thin Films of $CuAlO_2$. Nature 1997, 389 (6654), 939–942.
(2) Sun, H.; Arab Pour Yazdi, M.; Briois, P.; Pierson, J.-F.; Sanchette, F.; Billard, A. Towards Delafossite Structure of Cu–Cr–O Thin Films Deposited by Reactive Magnetron Sputtering: Influence of Substrate Temperature on Optoelectronics Properties. Vacuum 2015, 114, 101–107.
(3) Bera, A.; Deb, K.; Chattopadhyay, K. K.; Thapa, R.; Saha, B. Mixed Phase Delafossite Structured p Type $CuFeO_2$/CuO Thin Film on FTO Coated Glass and Its Schottky Diode Characteristics. Microelectron. Eng. 2016, 162, 23–26.
(4) Yu, M.; Draskovic, T. I.; Wu, Y. Cu(i)-Based Delafossite Compounds as Photocathodes in p-Type Dye-Sensitized Solar Cells. Phys. Chem. Chem. Phys. 2014, 16 (11), 5026–5033.
(5) Amrute, A. P.; Łodziana, Z.; Mondelli, C.; Krumeich, F.; Pérez-Ramírez, J. Solid-State Chemistry of Cuprous Delafossites: Synthesis and Stability Aspects. Chem. Mater. 2013, 25 (21), 4423–4435.
(6) Marquardt, M. A.; Ashmore, N. A.; Cann, D. P. Crystal Chemistry and Electrical Properties of the Delafossite Structure. Thin Solid Films. 2006, 496 (1), 146–156.
(7) Barnabe, A.; Thimont, Y.; Lalanne, M.; Presmanes, L.; Tailhades, P. p-Type Conducting Transparent Characteristics of Delafossite Mg-Doped $CuCrO_2$ Thin Films Prepared by RF-Sputtering. J. Mater. Chem. C 2015, 3 (23), 6012–6024.
(8) Galakhov, V. R.; Poteryaev, A. I.; Kurmaev, E. Z.; Anisimov, V. I.; Bartkowski, S.; Neumann, M.; Lu, Z. W.; Klein, B. M.; Zhao, T.-R. Valence-Band Spectra and Electronic Structure of $CuFeO_2$. Phys. Rev. B 1997, 56 (8), 4584–4591.
(9) Jiang, T.; Li, X.; Bujoli-Doeuff, M.; Gautron, E.; Cario, L.; Jobic, S.; Gautier, R. Modulation of Defects in Semiconductors by Facile and Controllable Reduction: The Case of p-Type $CuCrO_2$ Nanoparticles. Inorg. Chem. 2016, 55 (15), 7729–7733.
(10) Miura, A.; Lowe, M.; Leonard, B. M.; Subban, C. V.; Masubuchi, Y.; Kikkawa, S.; Dronskowski, R.; Hennig, R. G.; Abruña, H. D.; DiSalvo, F. J. Silver Delafossite Nitride, AgTaN2. J. Solid State Chem. 2011, 184 (1), 7–11.
(11) Yang, M.; Zakutayev, A.; Vidal, J.; Zhang, X.; Ginley, D. S.; DiSalvo, F. J. Strong Optical Absorption in $CuTaN_2$ Nitride Delafossite. Energy Environ. Sci. 2013, 6 (10), 2994–2999.
(12) Zakutayev, A.; Allen, A. J.; Zhang, X.; Vidal, J.; Cui, Z.; Lany, S.; Yang, M.; DiSalvo, F. J.; Ginley, D. S. Experi-

mental Synthesis and Properties of Metastable $CuNbN_2$ and Theoretical Extension to Other Ternary Copper Nitrides. Chem. Mater. 2014, 26 (17), 4970–4977.
(13) Liu, X.; Krott, M.; Müller, P.; Hu, C.; Lueken, H.; Dronskowski, R. Synthesis, Crystal Structure, and Properties of MnNCN, the First Carbodiimide of a Magnetic Transition Metal. Inorg. Chem. 2005, 44 (9), 3001–3003.
(14) Liu, X.; Stork, L.; Speldrich, M.; Lueken, H.; Dronskowski, R. FeNCN and $Fe(NCNH)_2$: Synthesis, Structure, and Magnetic Properties of a Nitrogen-Based Pseudo-Oxide and -Hydroxide of Divalent Iron. Chem. – Eur. J. 2009, 15 (7), 1558–1561.
(15) Krott, M.; Liu, X.; Fokwa, B. P. T.; Speldrich, M.; Lueken, H.; Dronskowski, R. Synthesis, Crystal-Structure Determination and Magnetic Properties of Two New Transition-Metal Carbodiimides: CoNCN and NiNCN. Inorg. Chem. 2007, 46 (6), 2204–2207.
(16) Liu, X.; Wankeu, M. A.; Lueken, H.; Dronskowski, R. A Novel Method for Synthesizing Crystalline Copper Carbodiimide, CuNCN. Structure Determination by X-Ray Rietveld Refinement. Z. Für Naturforschung B 2005, 60 (6), 593–596.
(17) Ressnig, D.; Shalom, M.; Patscheider, J.; More, R.; Evangelisti, F.; Antonietti, M.; Patzke, G. R. Photochemical and Electrocatalytic Water Oxidation Activity of Cobalt Carbodiimide. J. Mater. Chem. A 2015, 3 (9), 5072–5082.
(18) Odobel, F.; Pellegrin, Y. Recent Advances in the Sensitization of Wide-Band-Gap Nanostructured p-Type Semiconductors. Photovoltaic and Photocatalytic Applications. J. Phys. Chem. Lett. 2013, 4 (15), 2551–2564.
(19) Odobel, F.; Pellegrin, Y.; Gibson, E. A.; Hagfeldt, A.; Smeigh, A. L.; Hammarström, L. Recent Advances and Future Directions to Optimize the Performances of p-Type Dye-Sensitized Solar Cells. Coord. Chem. Rev. 2012, 256 (21–22), 2414–2423.
(20) Odobel, F.; Le Pleux, L.; Pellegrin, Y.; Blart, E. New Photovoltaic Devices Based on the Sensitization of p-Type Semiconductors: Challenges and Opportunities. Acc. Chem. Res. 2010, 43 (8), 1063–1071.
(21) Perera, I. R.; Daeneke, T.; Makuta, S.; Yu, Z.; Tachibana, Y.; Mishra, A.; Bäuerle, P.; Ohlin, C. A.; Bach, U.; Spiccia, L. Application of the Tris(acetylacetonato)iron(III)/(II) Redox Couple in p-Type Dye-Sensitized Solar Cells. Angew. Chem. Int. Ed. 2015, 54 (12), 3758–3762.
(22) Nattestad, A.; Mozer, A. J.; Fischer, M. K. R.; Cheng, Y.-B.; Mishra, A.; Bauerle, P.; Bach, U. Highly Efficient Photocathodes for Dye-Sensitized Tandem Solar Cells. Nat Mater 2010, 9 (1), 31–35.
(23) Dini, D.; Halpin, Y.; Vos, J. G.; Gibson, E. A. The Influence of the Preparation Method of NiO_x Photocathodes on the Efficiency of p-Type Dye-Sensitized Solar Cells. Coord. Chem. Rev. 2015, 304–305, 179–201.
(24) Xiang, H.; Dronskowski, R.; Eck, B.; Tchougréeff, A. L. Electronic and Magnetic Structure of Transition-Metal Carbodiimides by Means of GGA+U Theory. J. Phys. Chem. A 2010, 114 (46), 12345–12352.
(25) J. van Elp, J.; Eskes, H.; Kuiper, P.; Sawatzky, G. A. Electronic Structure of Li-Doped NiO. Phys. Rev. B 1992, 45 (4), 1612–1622.
(26) Schuler, T. M.; Ederer, D. L.; Itza-Ortiz, S.; Woods, G. T.; Callcott, T. A.; Woicik, J. C. Character of the Insulating State in NiO: A Mixture of Charge-Transfer and Mott-Hubbard Character. Phys Rev B 2005, 71 (11), 115113.
(27) Krott, M.; Liu, X.; Müller, P.; Dronskowski, R. Synthesis and Structure Determination of $Co(HNCN)_2$ and $Ni(HNCN)_2$. J. Solid State Chem. 2007, 180 (1), 307–312.
(28) Basin, A. S.; Kaplun, A. B.; Meshalkin, A. B.; Uvarov, N. F. The LiCl-KCl Binary System. Russ. J. Inorg. Chem. 2008, 53 (9), 1509–1511.
(29) Rodríguez-Carvajal, J. Recent Advances in Magnetic Structure Determination by Neutron Powder Diffraction. Phys. B Condens. Matter 1993, 192 (1), 55–69.
(30) Bérar, J.-F.; Lelann, P. E.s.d.'s and Estimated Probable Error Obtained in Rietveld Refinements with Local Correlations. J. Appl. Crystallogr. 1991, 24 (1), 1–5.
(31) BERAR, J. F. Acc. in Pow. Diff. II. NIST Sp Pub 1992, 846, 63.
(32) Farré, Y.; Zhang, L.; Pellegrin, Y.; Planchat, A.; Blart, E.; Boujtita, M.; Hammarström, L.; Jacquemin, D.; Odobel, F. Second Generation of Diketopyrrolopyrrole Dyes for NiO-Based Dye-Sensitized Solar Cells. J. Phys. Chem. C 2016, 120 (15), 7923–7940.
(33) Raissi, M.; Pellegrin, Y.; Jobic, S.; Boujtita, M.; Odobel, F. Infra-Red Photoresponse of Mesoscopic NiO-Based Solar Cells Sensitized with PbS Quantum Dot. Sci. Rep. 2016, 6, 24908.
(34) Kresse, G.; Furthmüller, J. Efficiency of Ab-Initio Total Energy Calculations for Metals and Semiconductors Using a Plane-Wave Basis Set. Comput. Mater. Sci. 1996, 6 (1), 15–50.
(35) Perdew, J. P.; Burke, K.; Wang, Y. Generalized Gradient Approximation for the Exchange-Correlation Hole of a Many-Electron System. Phys Rev B 1996, 54 (23), 16533–16539.
(36) The Perdew–Burke–Ernzerhof Exchange-Correlation Functional Applied to the G2-1 Test Set Using a Plane-Wave Basis Set. J. Chem. Phys. 2005, 122 (23), 234102.
(37) Péan, E.; Vidal, J.; Jobic, S.; Latouche, C. Presentation of the PyDEF Post-Treatment Python Software to Compute Publishable Charts for Defect Energy Formation. Chem. Phys. Lett. 2017, 671, 124–130.
(38) Wang, L.; Tao, M. Fabrication and Characterization of p-n Homojunctions in Cuprous Oxide by Electrochemical Deposition. Electrochem. Solid-State Lett. 2007, 10 (9), H248–H250.
(39) Das, B.; Renaud, A.; Volosin, A. M.; Yu, L.; Newman, N.; Seo, D.-K. Nanoporous Delafossite CuAlO2 from Inorganic/Polymer Double Gels: A Desirable High-Surface-Area p-Type Transparent Electrode Material. Inorg. Chem. 2015, 54 (3), 1100–1108.
(40) Renaud, A.; Chavillon, B.; Le Pleux, L.; Pellegrin, Y.; Blart, E.; Boujtita, M.; Pauporte, T.; Cario, L.; Jobic, S.; Odobel, F. $CuGaO_2$: A Promising Alternative for NiO in p-Type Dye Solar Cells. J. Mater. Chem. 2012, 22 (29), 14353–14356.

(41) Jiang, T.; Bujoli-Doeuff, M.; Farre, Y.; Blart, E.; Pellegrin, Y.; Gautron, E.; Boujtita, M.; Cario, L.; Odobel, F.; Jobic, S. Copper Borate as a Photocathode in p-Type Dye-Sensitized Solar Cells. RSC Adv. 2016, 6 (2), 1549–1553.

(42) Ginj Stands for the Injection Gibbs Free Energy. It Was Calculated from $\Delta G_{inj} = E_{VB}(NiCN_2) - E_{oo}(Dye^*) - E(dye/Dye^-) = 0.9 - 2.26 + 1.27 = -0.09$ eV.

Synopsis/TOC

Nickel carbodiimide ($NiCN_2$) crystallizes in the 2H delafossite structure type which is built upon infinite $^2/_\infty[NiN_2]$ layers connected by linear carbodiimides bridges $[N=C=N]^{2-}$. A XRD Rietveld refinement points out nickel deficiencies in the material, and band structure calculations carried out on the defect compound predict *p*-type conductivity in relation to a slight amount of N^{2-} localized in the vicinity of the Ni vacancies. This *p*-type conductivity is asserted by electrochemical impedance spectroscopy measurements.

